Future changes in extratropical storm tracks and baroclinicity under climate change

OPEN ACCESS

Future changes in extratropical storm tracks and baroclinicity under climate change

Jascha Lehmann[1,2]**, Dim Coumou**[1]**, Katja Frieler**[1]**, Alexey V Eliseev**[1,3,4] **and Anders Levermann**[1]

[1] Potsdam Institute for Climate Impact Research, Germany
[2] University of Potsdam, Germany
[3] A. M. Obukhov Institute of Atmospheric Physics RAS, Russia
[4] Kazan (Volga Region) Federal University, Russia

E-mail: jascha.lehmann@pik-potsdam.de

Abstract

The weather in Eurasia, Australia, and North and South America is largely controlled by the strength and position of extratropical storm tracks. Future climate change will likely affect these storm tracks and the associated transport of energy, momentum, and water vapour. Many recent studies have analyzed how storm tracks will change under climate change, and how these changes are related to atmospheric dynamics. However, there are still discrepancies between different studies on how storm tracks will change under future climate scenarios. Here, we show that under global warming the CMIP5 ensemble of coupled climate models projects only little relative changes in vertically averaged mid-latitude mean storm track activity during the northern winter, but agree in projecting a substantial decrease during summer. Seasonal changes in the Southern Hemisphere show the opposite behaviour, with an intensification in winter and no change during summer. These distinct seasonal changes in northern summer and southern winter storm tracks lead to an amplified seasonal cycle in a future climate. Similar changes are seen in the mid-latitude mean Eady growth rate maximum, a measure that combines changes in vertical shear and static stability based on baroclinic instability theory. Regression analysis between changes in the storm tracks and changes in the maximum Eady growth rate reveal that most models agree in a positive association between the two quantities over mid-latitude regions.

S Online supplementary data available from stacks.iop.org/ERL/9/084002/mmedia

Keywords: storm tracks, baroclinicity, climate change

Introduction

The day-to-day variability of weather in the mid-latitude regions is strongly affected by extratropical storm tracks. Storms in the northern mid-latitudes account for much of the total and extreme precipitation climatology (Hawcroft *et al* 2012, Pfahl and Wernli 2012) and the strong winds and potentially associated storm surges are among the major natural hazards in these regions (Leckebusch and

Ulbrich 2004, Pinto *et al* 2007, Schwierz *et al* 2009). Thus, the question of how extratropical storm tracks will change under global warming has been intensively analyzed in recent studies (Yin 2005, Bengtsson *et al* 2009, Ulbrich *et al* 2009, Catto *et al* 2011) with an emerging attention given to the analyses of multi-model ensembles (Ulbrich *et al* 2008, O'Gorman 2010, Chang *et al* 2012, Harvey *et al* 2012, 2013, Zappa *et al* 2013). Some authors have identified and analyzed individual cyclones and have shown that in the Northern Hemisphere (NH) the total number of cyclones are projected to decrease under climate change, whereas a potential increase exists for the number of extreme cyclones (Ulbrich *et al* 2009, Mizuta 2012, Zappa *et al* 2013). Other studies have used bandpass filtered measures of the storm tracks to

gain information about their changes on a global scale. Here, the largest consensus exists for a poleward and upward shift of the storm tracks in both hemispheres (Yin 2005, Chang *et al* 2012). Both diagnostic tools have furthermore been used to analyze the influence of different fields on the observed storm track changes, such as the horizontal temperature gradient, the upper-level zonal wind, the Eady growth rate, or ocean circulation changes (e.g. O'Gorman 2010, Mizuta 2012, Woollings *et al* 2012, Harvey *et al* 2013). However, there are still substantial differences in the projected storm track responses to climate change between different state-of-the-art climate models (Harvey *et al* 2012) and even larger uncertainties when it comes to the underlying mechanisms causing these storm track changes. In particular, the magnitude and sign of local storm track changes are in weak agreement between many individual model projections and the multi-model mean response (Ulbrich *et al* 2008, 2009, Harvey *et al* 2012).

This letter aims to contribute to the understanding of the storm track responses to climate change. Therefore, the latest generation of climate model projections from the Coupled Model Intercomparison Project Phase 5 (CMIP5) has been used to analyze the seasonal responses of extratropical storm tracks to future warming. We present historic and future changes (based on the emission scenario RCP8.5 (Moss *et al* 2010)) in winter and summer storm track activity of 22 CMIP5 models for both hemispheres. After a general assessment of the pattern of storm track changes, we analyze their influence on the seasonal cycle before we examine how the simulated storm track changes are associated with changes in the large-scale baroclinicity.

Data and methods

Daily-mean zonal and meridional wind speed data are used from all CMIP5 models for which the appropriate data were available at the time of writing. A list of the models is given in table S1 in the supplementary information (SI), available at stacks.iop.org/ ERL/9/084002/mmedia. The analysis is based on the time period 1950–2100, where 1950–2005 is based on historical forcing, and concatenated with 2006–2100 based on the high emissions scenario RCP8.5. We chose the scenario with the highest emission pathway, because we are interested in storm track changes under large global warming effects. In order to ensure comparability between models, only a single realization (the r1i1p1 run) from each model is used.

In this letter, storm tracks are estimated by the eddy kinetic energy (EKE) which is calculated for each individual month by applying a 2.5–6 day bandpass filter to the described daily wind field data. A similar approach was suggested by Blackmon (1976) for a 2–6 day bandpass range, and has been followed by several studies (e.g. Yin 2005, Ulbrich *et al* 2008, Harvey *et al* 2013). The EKE can hence be used as a measure for the interplay between the intensity and frequency of high and low pressure systems. The applied filter was developed by Murakami (Murakami 1979) and has been shown to produce accurate results (Christoph *et al* 1995,

Petoukhov *et al* 2008, Ren *et al* 2010). The difference between the applied 2.5–6 day bandpass filtering in this letter and the original 2–6 day bandpass range is likely to be minor, because only a relatively small amount of energy is in the 2–2.5 range (Randel and Held 1991). The EKE per unit volume is thereby simply calculated from

$$EKE = 0.5 \cdot \left(u'^2 + v'^2 \right)$$

where u' and v' are the band pass filtered zonal and meridional wind speeds. Subsequently, the EKE of each model is interpolated onto a common $2.5° \times 2.5°$ grid and a mass-weighted vertical average between 250 hPa and 850 hPa is applied. We define the seasonality in EKE as the difference in magnitude of mid-latitude mean EKE between winter and summer. Mid-latitude means are calculated by averaging EKE over all longitudes and between 35°–65°N for the NH and between 35°–65°S for the Southern Hemisphere (SH). The changes in EKE and the seasonality over time are given as relative changes with respect to the historical base period (1981–2000), where we focus on anomalies by the end of the 21st century (2081–2100). The 95% confidence interval and the statistical significance of the mean change in seasonality are derived for each model and the multi-model mean from a simple two-sample t-test.

In the second part of this study we analyze the relation between changes in EKE and changes in large-scale baroclinicity, represented by the maximum Eady growth rate (Lindzen and Farrell 1980, Hoskins and Valdes 1990). Changes in Eady growth rate are determined by changes in static stability and changes in vertical wind shear. Whilst static stability depends on the vertical potential temperature gradient, the vertical shear is closely related to the horizontal temperature gradient via the thermal wind equation. To analyze the influence of vertical shear on storm track changes compared to contributions from static stability, we also analyze the relation between EKE and vertical shear.

In this letter, we only present results for the analysis of the Eady growth rate. However, differences to the analysis of the vertical shear, calculated between 250–850 hPa, are discussed in the text and equivalent figures are given in the SI. The maximum Eady growth rate is defined as

$$\sigma_{BI} = 0.31 \cdot \frac{|f|}{N} \cdot \left| \frac{dV}{dz} \right|$$

where f is the Coriolis parameter, N the Brunt-Väisälä frequency, V the horizontal wind vector and z the vertical height. We calculate this quantity between 250–850 hPa. To assess the relationship between storm tracks and Eady growth rate, a linear regression is applied between both quantities at each grid point and for each model and season. To gain information about the correlation of the year-to-year variability of the storm tracks and the Eady growth rate, the time series are detrended before the regression analysis by subtracting the smoothed mean value with a half-width of 30 years. The same calculation is then repeated, but this time including all twelve months and without the detrending and the seasonal averaging process. The latter regression analysis
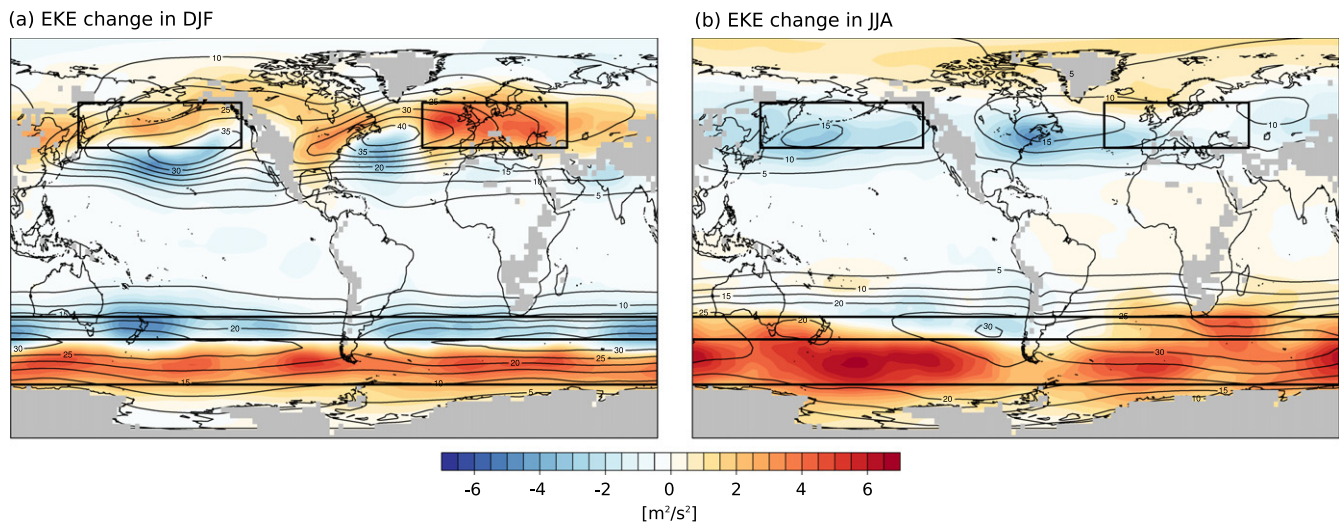
(a) EKE change in DJF

(b) EKE change in JJA

Figure 1. Projected storm track changes under future climate conditions represented by the difference in multi-model mean EKE (m^2/s^2) between the end of the 21st century (2081–2100) and the 20th century (1981–2000) for (a) DJF season and (b) JJA season. Contours of the 20th century EKE are shown in black, and regions of land higher than 1 km have been masked. Four regions of large EKE changes have been framed with black rectangles.

therefore describes the association between the seasonal cycle of EKE and the seasonal cycle of Eady growth rate.

Spatial pattern of storm track changes

Figure 1 shows the response of the multi-model mean EKE to climate change. During the northern winter (December-January-February (DJF)), the storm tracks shift polewards in the SH indicated by a reduction in EKE over the subtropics and an intensification southwards of the peak in the historical EKE. In the NH, the most prominent reductions in EKE are confined to the subtropical Atlantic and Pacific region and the strongest intensification can be seen over the North-East Atlantic, Eurasia, the North Pacific, and North America. In contrast, EKE changes during June-July-August (JJA) are rather uniform in each hemisphere. Here, the NH exhibits a general decrease in EKE in the mid-latitudes, with the greatest reduction over the Atlantic and Pacific Ocean basin, and a strong increase over the SH mid-latitudes. The pattern of EKE changes are similar across different altitudes of the troposphere, with the only exception of the northern winter. Here, the strongest differences can be seen at high latitudes between changes in the vertically averaged EKE and changes in EKE at 500 hPa (figure S1 in SI). In particular, EKE at 500 hPa exhibits negative changes in response to climate change over the North Pacific and North America. Also, changes in EKE during JJA are more consistent between the models than during DJF (figure S15 in SI).

Our results are qualitatively similar to findings from other studies which use similar diagnostic tools (O'Gorman 2010, Chang *et al* 2012, Harvey *et al* 2013). However, notable differences in the pattern of EKE changes can again be seen during DJF over North America and Eastern Europe. Here, the response of EKE seems to be sensitive to the applied diagnostic tool and the vertical height.

Storm track seasonality

After this general assessment of seasonal EKE responses, the mid-latitude means of EKEs are used to analyze changes in the seasonality in both hemispheres. Figure 2 shows the evolution of changes in mid-latitude mean EKE and seasonality. In NH winter, the multi-model median EKE increases by 5% until the end of the 21st century (figure 2(a), blue line). In contrast, the multi-model median EKE weakens substantially during JJA with a peak reduction of −14% in the year 2100 (figure 2(a), black line). The SH exhibits a strong increase in multi-model median EKE during JJA (14%) and almost no change during DJF (2%). These changes in EKE result in an amplified seasonal cycle in both hemispheres, with the amplification increasing at a rate of roughly 2% per decade in the NH and 6% per decade in the SH (figures 2(a) and (b), red line).

The enhanced seasonality in both hemispheres is a robust projection across all models (figure 3). For the NH, the relative change in seasonality predicted by individual models is close to the value of the multi-model mean, except for one model (GFDL-CM3). For this model, the historical seasonality is exceptionally small compared to the other models (see figure S8 in SI). In the SH, the inter-model spread is generally larger. This is mainly due to the chosen representation of the change in seasonality relative to the historical period, which is about three times smaller in magnitude in the SH than in the NH. Therefore small absolute changes in SH seasonality can lead to large relative changes and large confidence intervals, as can be seen in figure 3. However, an enhanced seasonality is evident in both hemispheres in all models, leading to a statistically significant increase in seasonality at the 95% confidence interval for the multi-model mean. The amplification at the end of the century is about four times stronger in the SH (92%, figure 3(b)) than in the NH (23%, figure 3(a)). However, the seasonal cycle of EKE is about three times
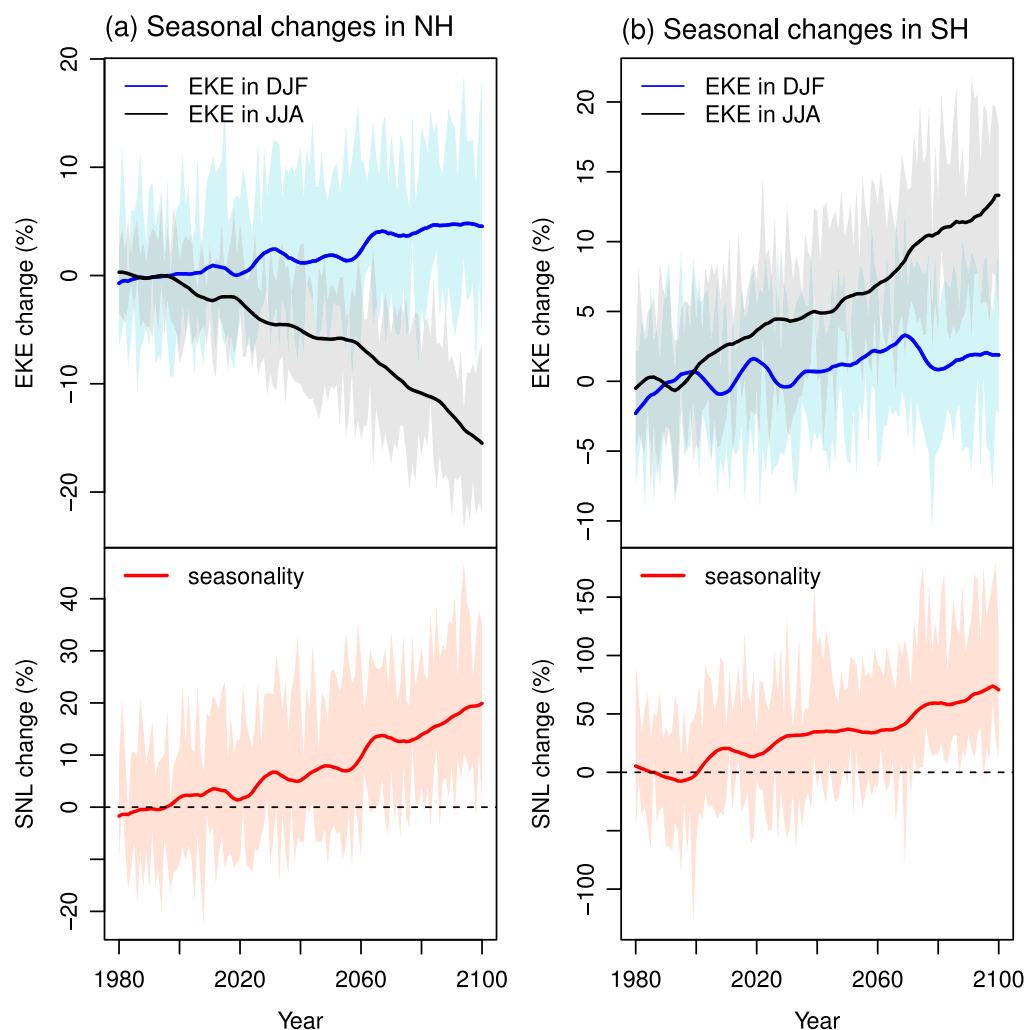
Figure 2. Changes in mid-latitude mean EKE shown separately for the (a) NH and (b) SH. The upper panel of each figure shows the time evolution of mid-latitude mean EKE changes during DJF (blue line) and JJA (black line). The evolution is given relative to the historical base period (1981–2000). Both lower panels show the change in seasonality (SNL), again given relative to the magnitude of the historical seasonal cycle. In all figures the shaded area reflects the interquartile range of the model spread and the thick solid line depicts the smoothed median value with a half-width of 8 years.

larger in the NH than in the SH, implying that in absolute terms the projected changes in seasonality are comparable between the two hemispheres.

We tested the sensitivity of our results to the vertical pressure level, which revealed that notable differences in the trends of mid-latitude mean EKE changes are only evident in NH winter and this is consistent with results from the spatial pattern of EKE changes at different altitudes (see figures S2–S7 in SI). However, the amplification of the seasonal cycle in both hemispheres is a robust feature across the troposphere.

Atmospheric dynamics

Figure 4 shows the seasonal changes of the mid-latitude mean Eady growth rate as presented in figure 3 for EKE. Similar trends between both quantities can be seen in each hemisphere and season. In the NH, the increase in EKE during DJF

(5%, figure 2(a)) is associated with an analogous increase in the multi-model median Eady growth rate (7%, figure 4(a)). During JJA, both quantities show a decrease over the 21st century (Eady growth rate, −4%). In the SH, the multi-model median Eady growth rate exhibits a weak amplification during DJF (3%, figure 4(b)), but increases substantially during JJA (7%, figure 4(b)), consistent with projected changes in EKE.

We also find similar changes in the mid-latitude mean vertical shear (figure S9 in SI). However, the strongest differences can be seen during southern summer, where the multi-model median vertical shear increases by 7% until the 21st century, whereas both EKE and Eady growth rate show almost no change. This difference can be explained by the influence of static stability on baroclinicity. Whereas vertical shear increases more or less homogeneously in the SH mid-latitudes, changes in Eady growth rate show a dipole pattern with a decrease at the equatorward side and an increase at the poleward side (similar to EKE, figure 1). Thus, an increase in static stability counterbalances the increase in vertical shear
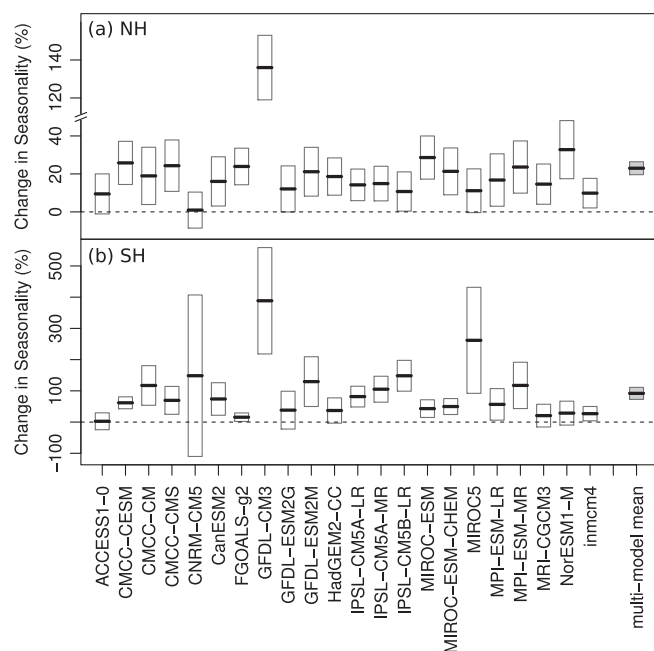
Figure 3. Change in seasonality of mid-latitude mean EKE under global warming. This is shown for the (a) NH and (b) SH. For each model and the multi-model mean, the mean value of the seasonality change is shown as a thick vertical line and the 95% confidence level is shown as a box. Both quantities were derived from a two-sample t-test, based on the last 20 years of the 20th and 21st centuries.

and therefore the mid-latitude mean EKE is almost unaffected.

Consistent with findings for mid-latitude mean EKE, the projected trends in mid-latitude mean vertical shear are qualitatively similar between the upper and lower troposphere, except for northern winter. Here, the multi-model median vertical shear increases in the upper troposphere (between 250 hPa and 500 hPa) but decreases in the lower troposphere (between 500 hPa and 850 hPa, figures S10–S11 in SI). This agrees well with changes in the horizontal temperature gradient, which are projected to increase in the upper troposphere, but decrease in the lower troposphere during northern winter (e.g. Harvey *et al* 2013). For the full troposphere this therefore yields only small relative changes in mid-latitude mean vertical shear, Eady growth rate, and EKE during northern winter, with the latter being consistent with findings from O'Gorman (2010).

Our results suggest that mid-latitude mean changes in Eady growth rate drive changes in EKE. To quantitatively analyze this relationship, we assess how the year-to-year variabilities of both quantities are correlated by applying a regression analysis between seasonally averaged and detrended time series of EKE and Eady growth rate.

Figure 5 shows the ratio between the number of models which exhibit a positive and those which exhibit a negative regression slope. Thus, a ratio of one implies that all models exhibit a positive correlation between EKE and Eady growth rate and a ratio of zero indicates that all models show a negative correlation. To highlight the storm track relevant regions, areas outside of the mid-latitudinal belt between 35°–65°N and 35°–65°S are shown semi-transparently.

In both hemispheres, large regions with positive regression slopes are evident during both seasons. These regions are primarily found over the mid-latitudes, i.e. regions of high EKE values (see contours in figure 1). In the NH mid-latitudes, the year-to-year variability of EKE during JJA (figure 5(b)) is especially well correlated with the year-to-year variability of Eady growth rate. Here, almost all models show a positive correlation (red shading) and most models have a statistically significant correlation at 95% confidence (stippling). During DJF, most models agree in a significant positive relation between EKE and Eady growth rate over the North Pacific. Model agreement is somewhat weaker over parts of North America and the western North Atlantic. This is probably related to the uncertainty in the projected EKE changes during northern winter over this region (see figure 1 and figure S1 in SI). Strictly speaking, based on baroclinic theory one would not necessarily expect a point-to-point correlation between EKE and baroclinicity. Baroclinic theory tells that small disturbances grow to large amplitudes along sufficiently (1000 s of km) long baroclinic zones. Thus, downstream of such baroclinic zones EKE can still be large although baroclinicity weakens, which might be a reason for the weak agreement over Eurasia. Over the (sub-) tropics there are large regions that indicate a negative relation between EKE and Eady growth rate. This can be explained by very low magnitudes of EKE and Eady growth rate in these latitudes, which lead to high uncertainties in the estimated regression slopes, that vary around zero. This is confirmed by the multi-model mean regression slope which is close to zero in most parts of the (sub-) tropics (see figure S13 in SI).

In the SH summer (figure 5(a)), a positive and, for most models, significant correlation between EKE and Eady growth rate exists over an area around New Zealand and over a zonal band between 50°–65°S. During JJA, the regression pattern looks similar. For both seasons, there is weaker agreement between EKE and Eady growth rate around 45°S, which is exactly at the core of the storm track. Speculatively, non-linear effects due to saturation of EKE play a role, such that an increase in Eady growth rate does not lead to a linear increase in EKE. Regression analysis of EKE and vertical shear (figure S14 in SI) shows similar patterns of model agreement for both hemispheres and both seasons. This implies that Eady growth rate, but also vertical shear by itself, can explain much of the year-to-year changes in EKE over the mid-latitudes.

Strong changes in EKE and Eady growth rate are not only seen in the year-to-year variability but also during the course of a year (figure S12 in SI). We therefore also regressed the changes in EKE and Eady growth rate due to their seasonal cycle against each other. Figure 6 shows the spatially averaged regression slopes for four chosen regions with especially strong changes in EKE over the 21st century. The region borders are shown in figures 1 and 4, and are defined for Europe (Europe: 40°–60°N, 30°W–50°E), the North Pacific (NH.Pacific: 40°–60°N, 140°E–120°W), and two zonal bands in the SH (SH.35°–45°: 35°–45°S, 180°W–180°E and SH.45°–65°: 45°–65°S, 180°W–180°E). For each region, the multi-model mean and the inter-model spread
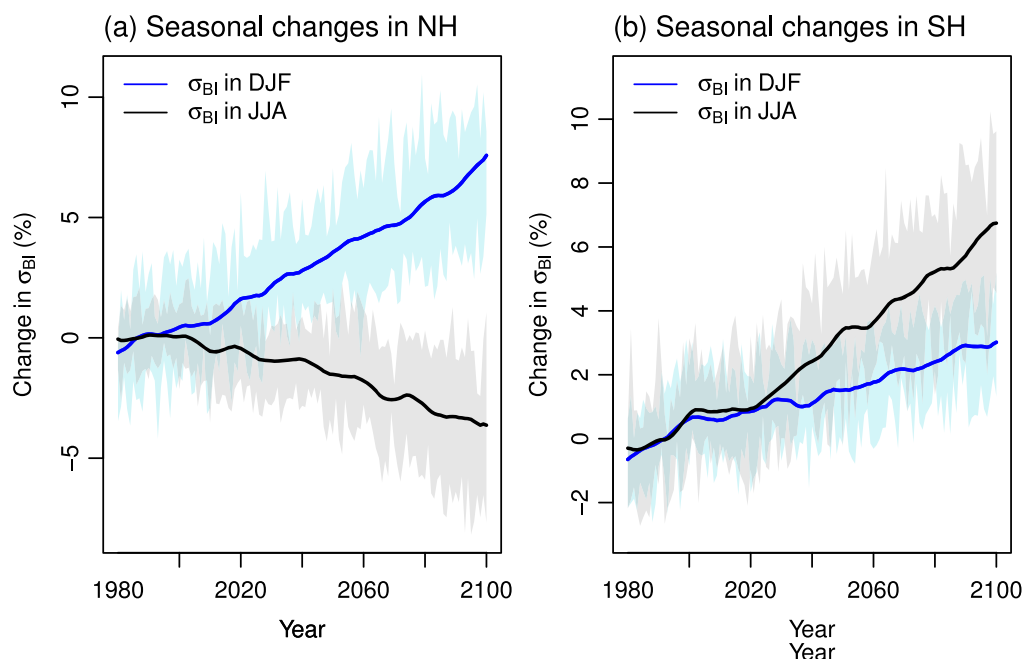
Figure 4. Changes in mid-latitude mean Eady growth rate separately shown for the (a) NH and (b) SH as in figure 3 for EKE.

of the regionally averaged regression slope is shown for regression of the year-to-year variability during DJF (dark blue boxes) and JJA (light blue boxes) and regression of the seasonal cycle (yellow boxes).

Within all four regions, the magnitudes of the regression slopes are in general agreement across the different regression methods, as indicated by the overlapping ranges of the full inter-model spread. Regression slopes from regressing the seasonal cycle are qualitatively similar to regression slopes from the year-to-year variability, but generally larger in magnitude. We suggest that these differences in the magnitude of the regression slopes between different regression methods can at least partly be explained by differences in the variability of Eady growth rate changes. Changes in Eady growth rate are much larger over the seasonal cycle (i.e. between summer and winter) than from year-to-year (i.e. from one summer to the next). Therefore, a regression using the full seasonal cycle covers a larger range in the input variable (i.e. Eady growth rate) and is thus less affected by regression dilution, which causes a bias in the regression slope towards zero. An estimate of the magnitude in variability is the standard deviation, which is shown for the multi-model mean Eady growth rate in figure 6 above each box and whisker symbol. These numbers suggest that without the bias caused by the regression dilution we could expect to see even stronger agreements in the regression slopes between the methods.

Conclusion and discussion

This letter has analyzed storm track changes under the RCP8.5 greenhouse gas emission scenario. The storm tracks are represented by EKE which we calculated from bandpass filtered daily-mean zonal wind from 22 different CMIP5 models. In the first section, the change in seasonality, i.e. the difference in magnitude between winter and summer EKE, has been studied in detail. Afterwards, a linear regression model has been applied to EKE and Eady growth rate to analyze how changes in EKE are related to changes in large-scale baroclinicity.

The pattern of multi-model mean storm track responses to climate change is different in each hemisphere, and between winter and summer seasons. Whereas most studies focus on the stronger winter time storm tracks, here we show that for the mid-latitude mean storm tracks, CMIP5 models project a large and consistent change in EKE in both hemispheres during JJA, which implies a larger seasonality in a future climate. The latter is in agreement with previous analysis based on CMIP3 models (O'Gorman 2010). The amplified seasonal cycle is a robust feature across all models, and leads to a significant increase in seasonality of the multi-model mean at the 95% confidence interval in both hemispheres. This implies that whereas the SH exhibits an amplification of the stronger winter storm tracks, the largest relative changes in the NH are expected during summer, where CMIP5 models project a robust weakening of the storm tracks.

Similar trends are also evident for changes in the mid-latitude mean Eady growth rate. This suggests, that mid-latitude mean changes in Eady growth rates drive changes in EKE. The Eady growth rate is a suitable measure of baroclinicity and describes the potential of small perturbations to develop into larger storms. It is thus a good predictor for EKE at the early stage of storm evolution, but might be less applicable for later stages. Nevertheless, regression analysis reveals that in both seasons there are large regions where models agree on a positive correlation between the year-to-
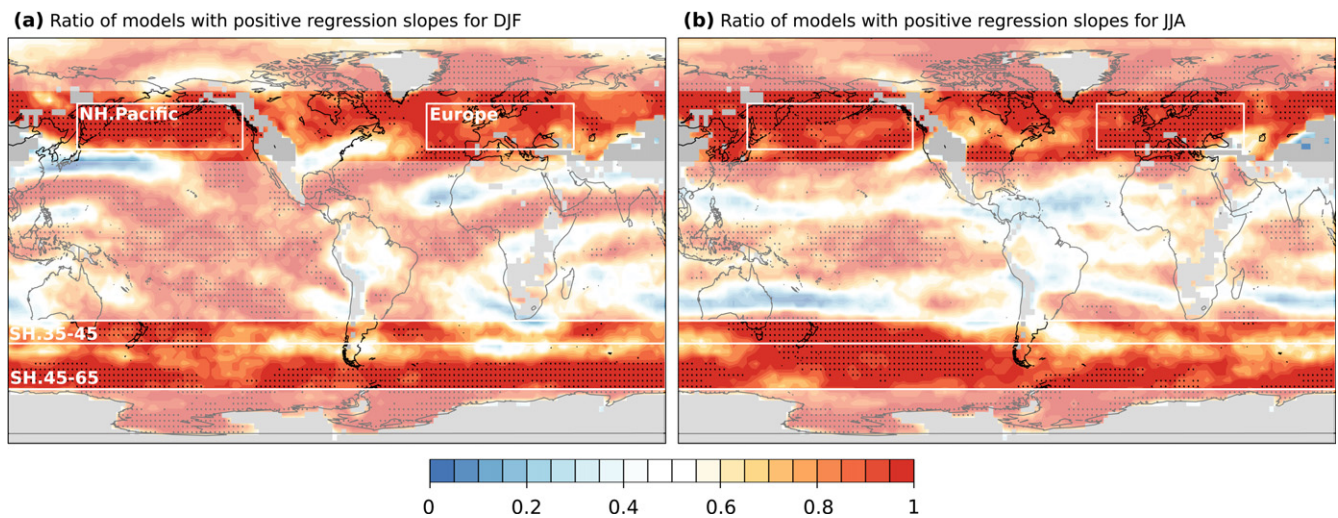
Figure 5. Model agreement on positive or negative regression coefficients. Colours indicate the ratio between the number of models showing positive (red shading) or negative (blue shading) regression coefficients, derived from linear regression analysis between the seasonally averaged and detrended time series of EKE and Eady growth rate in (a) DJF and (b) JJA. Stippling indicates regions where more than 50% of the models exhibit regression slopes that are significant at the 95% confidence level, as indicated by a corresponding p-value < 0.05. Regions outside of the zonal bands between 35°–65°N and 35°–65°S are shown semi-transparently and regions with topography above 1 km have been masked in grey. White boxes illustrate the regions used for the detailed regression analysis (see figure 6).
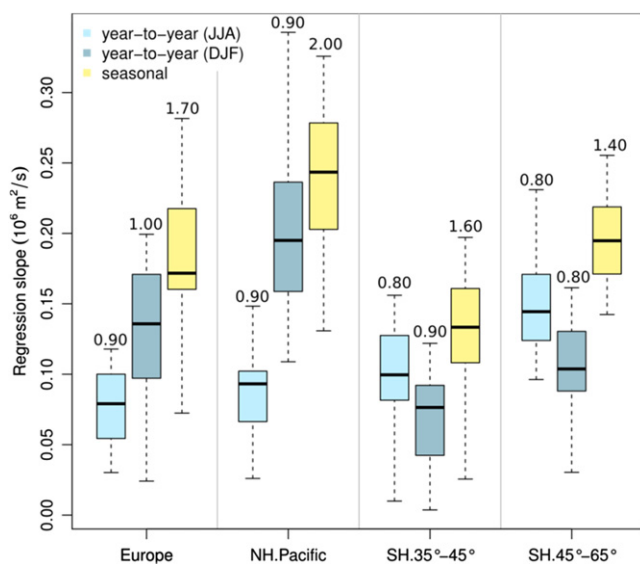

Figure 6. Regression slopes of different regions for both regression methods. Results from regressing the year-to-year variability between EKE and vertical shear are coloured in light blue (JJA) and dark blue (DJF) and results from the regression analysis of the seasonal cycle are coloured in yellow. In each case, the box and whisker symbols indicate the median, the interquartile range and the extreme values of the inter-model spread. Above each box and whisker symbol the standard deviation (10^4 1/s) of the corresponding time series of the Eady growth rate is shown.

year variability in EKE and Eady growth rate. These regions are primarily found over the storm track relevant mid-latitudes, where more than half of the models exhibit significant correlations. Regression of the year-to-year variability between EKE and vertical shear yields similar results.

For the four chosen regions of large storm track changes (Europe, NH.Pacific, SH.35°–45°, SH.45°–65°), models agree in a strong correlation between the year-to-year

variability of EKE and the Eady growth rate. Regression analysis of the year-to-year variability and the variability due to changes associated with the seasonal cycle give similar regression slopes. This suggests that the relation between changes in Eady growth rate and EKE in different years is equivalent to the relation between changes driven by the seasonal cycle. Regression slopes are slightly larger for regressions of the seasonal cycle than for regressions of the year-to-year variability. We argue that this can at least partly be explained by the larger intra-annual variability in Eady growth rate, as compared to the inter-annual variability. Therefore, a regression using the full seasonal cycle is less affected by regression dilution than a regression using the year-to-year changes.

Our results are in general agreement with other studies using similar metrics to analyze contributing factors to the projected storm track changes under future climate conditions (Yin 2005, Pinto *et al* 2008, O'Gorman 2010, Ren *et al* 2010, Wu *et al* 2010, Mizuta 2012, Harvey *et al* 2013). However, comparability is difficult, as most studies focus on the association of climatological changes due to global warming. This letter, on the other hand, analyzes the correlation of the year-to-year variability and the correlation of the seasonal cycle. Vertical shear and static stability mainly determine the baroclinicity in the atmosphere. Our results show that over the storm track relevant regions, Eady growth rate can explain much of the projected storm track changes. In addition, we find that storm track variability is dominated by changes in shear, and that the shear alone can statistically explain the changes in EKE in some seasons. This presumption is supported by results from Ren *et al* (2010) who find that during winter and summer, baroclinicity is mainly determined by the vertical shear over two regions confined to the North Pacific and Central Asia.

We showed that CMIP5 models project a robust weakening of EKE and associated storm tracks in boreal summer. Storms bring moist and cool air from the oceans to the continents and thus a weakening of storm tracks could possibly lead to more prolonged heat waves or droughts in the midlatitudes. We will study this possible relation in future research.

Acknowledgments

References

Bengtsson L, Hodges K I and Keenlyside N 2009 Will extratropical storms intensify in a warmer climate? *J. Clim.* **22** 2276–301

Blackmon M 1976 A climatological spectral study of the 500 mb geopotential height of the Northern Hemisphere *J. Atmos. Sci.* **33** 1607–23

Catto J L, Shaffrey L C and Hodges K I 2011 Northern hemisphere extratropical cyclones in a warming climate in the HiGEM high resolution climate model *J. Clim.* **24** 5336–52

Chang E K M, Guo Y and Xia X 2012 CMIP5 multimodel ensemble projection of storm track change under global warming *J. Geophys. Res.* **117** (D23)D23118

Christoph M, Ulbrich U and Haak U 1995 Faster determination of the intraseasonal variability of storm tracks using Murakami's recursive filter *Mon. Weather Rev.* **123** 578–81

Harvey B J, Shaffrey L C, Woollings T J, Zappa G and Hodges K I 2012 How large are projected 21st century storm track changes? *Geophys. Res. Lett.* **39** 1–5

Harvey B J, Shaffrey L C and Woollings T J 2013 Equator-to-pole temperature differences and the extra-tropical storm track responses of the CMIP5 climate models *Clim. Dyn.* doi:10.1007/s00382-013-1883-9

Hawcroft M K, Shaffrey L C, Hodges K I and Dacre H F 2012 How much Northern Hemisphere precipitation is associated with extratropical cyclones? *Geophys. Res. Lett.* **39** L24809

Hoskins B and Valdes P 1990 On the existence of storm-tracks *J. Atmos. Sci.* **47** 1854–64

Leckebusch G C and Ulbrich U 2004 On the relationship between cyclones and extreme windstorm events over Europe under climate change *Glob. Planet. Change* **44** 181–93

Lindzen R and Farrell B 1980 A simple approximate result for the maximum growth rate of baroclinic instabilities *J. Atmos. Sci.* **37** 1648–54

Mizuta R 2012 Intensification of extratropical cyclones associated with the polar jet change in the CMIP5 global warming projections *Geophys. Res. Lett.* **39** L19707

Moss R H *et al* 2010 The next generation of scenarios for climate change research and assessment *Nature* **463** 747–56

Murakami M 1979 Large-scale aspects of deep convective activity over the GATE area *Mon. Weather Rev.* **107** 994–1013

O'Gorman P A 2010 Understanding the varied response of the extratropical storm tracks to climate change *Proc. Natl. Acad. Sci. USA* **107** 19176–80

Petoukhov V, Eliseev A V, Klein R and Oesterle H 2008 On statistics of the free-troposphere synoptic component: an evaluation of skewnesses and mixed third-order moments contribution to the synoptic-scale dynamics and fluxes of heat and humidity *Tellus* A **60** 11–31

Pfahl S and Wernli H 2012 Quantifying the relevance of cyclones for precipitation extremes *J. Clim.* **25** 6770–80

Pinto J G, Fröhlich E L, Leckebusch G C and Ulbrich U 2007 Changing European storm loss potentials under modified climate conditions according to ensemble simulations of the ECHAM5/MPI-OM1 GCM *Nat. Hazards Earth Syst. Sci.* **7** 165–75

Pinto J G, Zacharias S, Fink A H, Leckebusch G C and Ulbrich U 2008 Factors contributing to the development of extreme north atlantic cyclones and their relationship with the NAO *Clim. Dyn.* **32** 711–37

Randel W and Held I 1991 Phase speed spectra of transient eddy fluxes and critical layer absorption *J. Atmos. Sci.* **48** 688–97

Ren X, Yang X and Chu C 2010 Seasonal variations of the synoptic-scale transient eddy activity and polar front jet over East Asia *J. Clim.* **23** 3222–33

Schwierz C, Köllner-Heck P, Zenklusen Mutter E, Bresch D N, Vidale P-L, Wild M and Schär C 2009 Modelling european winter wind storm losses in current and future climate *Clim. Change* **101** 485–514

Ulbrich U, Pinto J G, Kupfer H, Leckebusch G C, Spangehl T and Reyers M 2008 Changing northern hemisphere storm tracks in an ensemble of IPCC climate change simulations *J. Clim.* **21** 1669–79

Ulbrich U, Leckebusch G C and Pinto J G 2009 Extra-tropical cyclones in the present and future climate: a review *Theor. Appl. Climatol.* **96** 117–31

Woollings T, Gregory J M, Pinto J G, Reyers M and Brayshaw D J 2012 Response of the North Atlantic storm track to climate change shaped by ocean–atmosphere coupling *Nat. Geosci.* **5** 313–7

Wu Y, Ting M, Seager R, Huang H-P and Cane M. a. 2010 Changes in storm tracks and energy transports in a warmer climate simulated by the GFDL CM2.1 model *Clim. Dyn.* **37** 53–72

Yin J H 2005 A consistent poleward shift of the storm tracks in simulations of 21st century climate *Geophys. Res. Lett.* **32** 2–5

Zappa G, Shaffrey L C, Hodges K I, Sansom P G and Stephenson D B 2013 A multi-model assessment of future projections of north atlantic and european extratropical cyclones in the CMIP5 climate models *J. Clim.* **26** 5846–62